

# Relative contributions of the Tibetan Plateau thermal forcing and the Indian Ocean Sea surface temperature basin mode to the interannual variability of the East Asian summer monsoon

Jun Hu · Anmin Duan

Received: 20 November 2014 / Accepted: 28 January 2015 / Published online: 10 February 2015  
© Springer-Verlag Berlin Heidelberg 2015

**Abstract** Investigating the relationships among different factors impacting the East Asian summer monsoon (EASM) is urgent for improving its predictability. In the present study, two factors, the Tibetan Plateau (TP) atmospheric thermal forcing and the Indian Ocean sea surface temperature basin mode (IOBM), are selected to compare their relative contributions to the interannual variability of the EASM. Both statistical methods and numerical experiments are used to separate and compare their respective influences under realistic circumstances. The results indicate that the IOBM mainly drives an anticyclonic anomaly over the northwestern Pacific in the lower troposphere, which is consistent with the dominant mode of the EASM circulation system. Meanwhile, influences from the TP thermal forcing are primarily on the anticyclonic anomaly over the TP in the upper troposphere, together with the enhanced southwesterly over southern China and a northerly anomaly over northern China in the lower troposphere. Moreover, the TP thermal forcing seems to play a more important role than the IOBM in affecting the main rainfall belt of the EASM, which extends from the middle and lower reaches of the Yangtze River to Japan. Such a rainfall pattern anomaly is directly related to the anomalous northerly over northern China and the resultant stronger moisture convergence over the main rainfall belt region when a

strong TP thermal forcing occurs. In addition, the IOBM can increase the precipitation over the southeastern TP during its positive phase and hence enhance the in situ atmospheric heat source to a certain degree.

**Keywords** Tibetan Plateau (TP) · Indian Ocean basin mode (IOBM) · East Asian summer monsoon (EASM) · Atmospheric thermal forcing · Summer rainfall

## 1 Introduction

The East Asian summer monsoon (EASM) is a complex monsoon system with hybrid characteristics of tropical and subtropical monsoon, which is distinct from the Indian summer monsoon (Ding and Chan 2005). Floods and droughts caused by an anomalous EASM often bring disaster to a region that is populated by nearly two billion people. Efforts to elucidate the underlying mechanisms and predict the interannual variability of the EASM have been ongoing for a long time. Many external factors, including the El Niño–Southern Oscillation (ENSO) (Fu and Teng 1988; Wang et al. 2000, 2008b; Chang et al. 2000; Yang and Lau 2006; Weng et al. 2007), Indian Ocean sea surface temperature (SST) (Yang et al. 2007; Xie et al. 2009; Wu et al. 2009a), snow cover/depth over the Tibetan Plateau (TP) (Wu and Qian 2003; Wu and Kirtman 2007; Zhao et al. 2007), surface sensible heating over the TP (Duan and Wu 2005; Duan et al. 2013; Wang et al. 2013), the Arctic sea ice (Huang et al. 1995; Zhao et al. 2004; Wu et al. 2009b), the Arctic Oscillation (AO) (Gong and Ho 2003; Gong et al. 2011) and Antarctic Oscillation (Nan and Li 2003; Nan et al. 2009; Zhu 2009), are known to have impacts on the interannual variability of the EASM to a certain degree. However, the predictability of the

J. Hu · A. Duan (✉)  
State Key Laboratory of Numerical Modeling for Atmospheric Sciences and Geophysical Fluid Dynamics (LASG), Institute of Atmospheric Physics (IAP), Chinese Academy of Sciences (CAS), P. O. Box 9804, Beijing 100029, China  
e-mail: amduan@lasg.iap.ac.cn

J. Hu  
Department of Earth Sciences, University of Southern California, Los Angeles, CA, USA

interannual variability of the EASM is still at a low level (Wang et al. 2009b). Perhaps one reason for this is the lack of understanding of the relationships among different contributing factors, and how their interactions influence such a complicated subtropical monsoon system. Most external factors impact the EASM through teleconnections, which are major sources of predictability (Wang et al. 2009b). Finding factors that contribute more to the EASM, and then evaluating and improving the capabilities of models in simulating the teleconnection patterns generated by these more important factors, may be a more efficient way to improve model skill in monsoon prediction. Also, the most important factors can be considered to establish useful empirical models for predictions (Wu et al. 2009c; Wang et al. 2013). Thus, comparing different impacts among many factors affecting the EASM is a key step to improving our understanding of the variability of the EASM, and its prediction.

Some previous studies have attempted to discuss the relative contributions of different factors affecting the Asian monsoon. For example, Yang and Lau (1998) found that the tropical eastern Pacific SST plays a more important role than the soil moisture of the Asian continent in the Asian summer monsoon. Gong and Ji (1998a, b) argued that the atmospheric heat source over the TP could influence the northwestern Pacific subtropical high, mainly by the frontal zone along its northern flank, while the heat source over the tropical northwestern Pacific primarily influences the easterly jet along its southern flank. Nevertheless, the relative contribution of land and ocean to the interannual variability of the EASM in terms of circulation and precipitation anomalies remains vague.

From the land–sea–air coupling perspective, and considering the very nature of the monsoon is a seasonal reversal of the land–sea thermal contrast, in the present study we choose two factors—the atmospheric heat source over the TP and the Indian Ocean SST basin mode (IOBM) (i.e. one land factor and one ocean factor)—to evaluate their relative contributions to the interannual variability of the EASM.

In summer, the atmospheric heat source over the TP is known to be one of the strongest heat sources in Eurasia, and has direct impacts on the variability of the EASM. Using a quasi-geostrophic model, Huang (1985) pointed out that an increase in the magnitude of the heat source over the TP would strengthen the ridge over the Okhotsk Sea. Later studies (Luo and Chen 1995; Zhao and Chen 2001; Duan and Wu 2005; Jian et al. 2004; Wang et al. 2014) revealed that when the TP atmospheric heat source is enhanced, precipitation will increase over the regions along the middle and lower reaches of the Yangtze and Huai rivers, while precipitation will decrease over the coastal region of southeastern China. Hsu and Liu (2003) further confirmed the close relationship between the dominant

mode of East Asian summer precipitation and the TP diabatic heating.

The IOBM, which is the dominant mode of the variability of Indian Ocean SST, is closely related to the variability of the EASM. Yang et al. (2007) indicated that the IOBM could act as a capacitor to prolong the influence of El Niño on the EASM, such as the enhancement of the northwestern Pacific high and the South Asian high during the positive phase of the IOBM. Moreover, warm Indian Ocean SST can excite a warm Kelvin wave in the lower atmosphere over the tropical ocean, which inhibits convection over the northwestern Pacific, thus strengthening the northwestern Pacific high (Wu et al. 2009a; Xie et al. 2009). Another possible mechanism for the IOBM's influence on the EASM is via warm Indian Ocean SST strengthening the local Hadley circulation between the Maritime Continent and the northwestern Pacific, resulting in more intense descending motion over the northwestern Pacific (Wu et al. 2009a; Zhu et al. 2014). We choose the IOBM in the present study as the main ocean mode because it is adjacent to the EASM region and has the closest simultaneous correlation with the EASM compared to the Indian Ocean dipole mode (IOD) and ENSO, as well as ENSO Modoki (Fig. 1). Also, its close correlation with the EASM is stable, sustaining from the previous winter to the current summer. In contrast, other ocean modes (e.g. the IOD) only correlate closely with the EASM in the previous autumn; the relationship quickly decreases over the following two seasons.

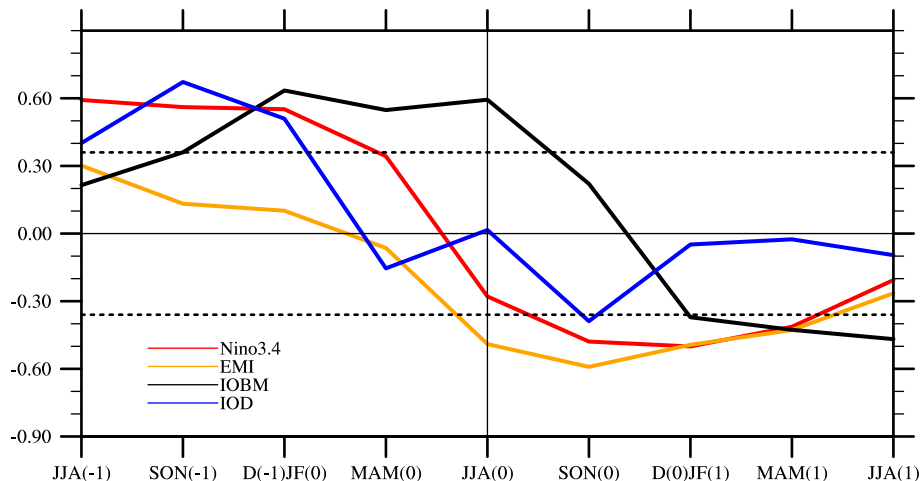
The remainder of the paper is organized as follows. Section 2 introduces the data, statistical methods, numerical model, and index definitions. In Sect. 3, the different contributions of the IOBM and TP thermal forcing are compared based on the observation data. Section 4 further confirms their relative contributions via the results of the numerical experiments. Section 5 explores the impact of the IOBM on the TP thermal forcing, and Sect. 6 concludes with a summary and further discussion of the key findings.

## 2 Data, methods, model and indexes

### 2.1 Data

The data used in this study comprise: the regular (four times daily) surface observations from 71 meteorological stations over the central and eastern TP provided by the China Meteorological Administration (CMA), as described in Duan and Wu (2008), in which the precipitation records have been corrected by the method recommended by Ye et al. (2004); satellite radiation data from Global Energy and Water Cycle Exchanges Project-Surface Radiation Budget (GEWEX-SRB) at the resolution of  $1^\circ \times 1^\circ$ ; precipitation from the Global Precipitation Climatology

**Fig. 1** Lead-lag correlation between the EASM index (Wang et al. 2008b) and four main ocean indexes [Niño 3.4 representing ENSO, EMI representing El Niño Modoki, Indian Ocean basin mode (IOBM), and Indian Ocean Dipole (IOD) mode] of different seasons. The two dashed lines represent the 95 % confidence level



Project version 2.1 (GPCP) (Adler et al. 2003) at the resolution of  $2.5^\circ \times 2.5^\circ$  and the Asian Precipitation—Highly-Resolved Observational Data Integration Towards Evaluation of Water Resource (APHRODITE, Yasutomi et al. 2011) at the resolution of  $0.5^\circ \times 0.5^\circ$ ; SST from the Hadley Center (Rayner et al. 2003) at the resolution of  $1^\circ \times 1^\circ$ ; and the Japanese 55-year Reanalysis (JRA-55, Ebina et al. 2011,  $1.25^\circ \times 1.25^\circ$ , 37 pressure levels), the latest reanalysis from the European Centre for Medium-Range Weather Forecasts (ECMWF), ERA-Interim (Dee et al. 2011,  $1.5^\circ \times 1.5^\circ$ , 37 pressure levels) and National Centers for Environmental Prediction and the Department of Energy for reanalysis datasets 2 (NCEP/DOE, Kanamitsu et al. 2002,  $1.875^\circ \times 1.9^\circ$ , 28 pressure levels) reanalysis data. The time range of all the datasets used in this study is 1979–2007, except SRB, which is only available from 1984 to 2007. Note that the linear trends in all data have been removed in advance to focus on the interannual variability.

## 2.2 Methods

Partial correlation (Zar 1998; Saji and Yamagata 2003) is used to compare the different contributions of the IOBM and TP thermal forcing. This method involves the correlation between two variables while eliminating the influence of a third variable, thus in this case enabling us to separate the contributions of the TP thermal forcing and IOBM more clearly than would otherwise be possible via the normal correlation coefficient. If the EASM index is marked as variable 1, the IOBM index as variable 2, and the TP thermal forcing as variable 3, then the correlation between the EASM index and IOBM index with the impacts of the TP thermal forcing removed is designated as  $r_{12,3}$ :

$$r_{12,3} = \frac{r_{12} - r_{13}r_{23}}{\sqrt{(1 - r_{13}^2)(1 - r_{23}^2)}},$$

where  $r_{ij}$  is the correlation between the variables  $i$  and  $j$ .

Multiple-variable linear regression is also employed to compare the relative contributions of the IOBM and TP thermal forcing. The two factors are regressed onto the EASM index or East Asian summer precipitation index (see the definitions in Sect. 2.4) and the standard coefficients can be explained as their relative contributions. Standard regression coefficients are calculated as follows. If  $x_1$  stands for the IOBM index,  $x_2$  for the TP thermal forcing, and  $y$  for the EASM index, we can first obtain their corresponding regression coefficients  $\hat{\beta}_i$  using the linear least squares method:

$$y = \hat{\beta}_1x_1 + \hat{\beta}_2x_2 + \hat{\beta}_0.$$

The standard regression coefficients  $b_i$  are then calculated using

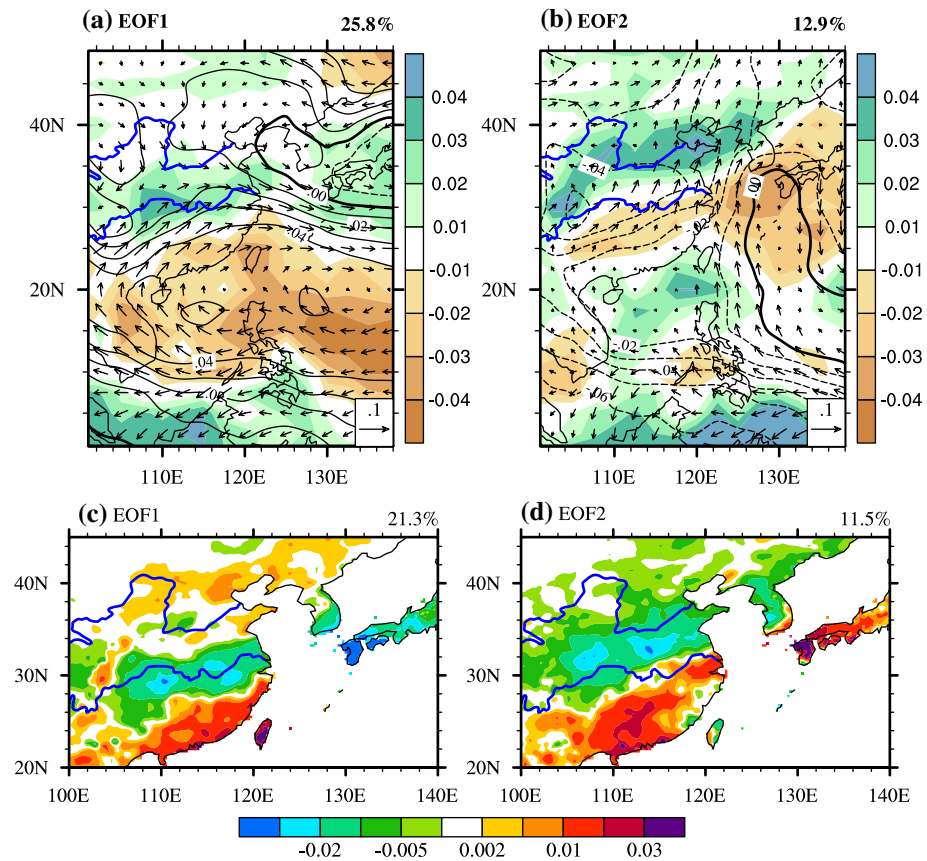
$$b_i = \hat{\beta}_i \frac{s_{x_i}}{s_y},$$

where  $s_{x_i}$  and  $s_y$  are the standard deviations of the time series of  $x_i$  and  $y$  respectively.

## 2.3 Model

The atmospheric general circulation model (AGCM) used in this study is the Finite-volume/Spectral Atmospheric Model (F/SAMIL) developed by the IAP/LASG (Institute of Atmospheric Physics/State Key Laboratory of Numerical Modeling for Atmospheric Sciences and Geophysical Fluid Dynamics) (Zhou et al. 2012, 2015; Yu et al. 2014). It comprises two versions: one with a spectral dynamical core (SAMIL) and another with a finite-volume dynamical core (FAMIL). These two versions share the following physical parameterizations. The mass flux cumulus parameterization of Tiedtke (1989) is employed to describe deep, mid-level and shallow convection, with a modified closure assumption

**Fig. 2** The first two leading modes of the MV-EOF of 850 hPa wind, precipitation and sea level pressure (**a, b**) (contours: sea level pressure; shading: precipitation; vectors: wind) and the first two leading modes of the EOF of East Asian summer precipitation based on APHRODITE datasets (1979–2007) (**c, d**). The blue curves represent the Yangtze River and Yellow River from south to north, and the black bold curve denotes the area above 1,500 m



and the formation of organized entrainment and detrainment (Nordeng 1994). The planetary boundary layer scheme is a non-local first-order closure scheme proposed by Holtslag and Boville (1993). For the effects of gravity wave drag, only orographic gravity waves are considered (Palmer et al. 1986). In FAMIL, the Rapid Radiative Transfer Model for GCMs (RRTMG) (Clough et al. 2005) is implemented instead of the Edwards–Slingo radiation scheme (Edwards and Slingo 1996; Sun 2011) in SAMIL. FAMIL uses a single moment cloud microphysics scheme (Harris and Lin 2014), while SAMIL employs a simple large-scale condensation scheme.

F/SAMIL is capable of simulating both the climate mean and interannual variability of monsoon (Wu et al. 1996), and has been successfully used in studies concerning the Asian monsoon and the role of the TP thermal forcing (e.g. Liu et al. 2004; Wu et al. 2012; Duan et al. 2013). In the present study we use the FAMIL version. FAMIL has various horizontal and vertical resolution options, among which we choose the horizontal resolution of C48 ( $1.875^\circ \times 1.875^\circ$ , ~200 km) and 32 vertical levels (top level is about 2.16 hPa).

#### 2.4 Indexes

To measure the variability of the EASM, we use the EASM index recommended by Wang et al. (2008b), which is the principal component of the first leading mode of the interannual variability of the EASM [derived by multi-variable empirical orthogonal function (EOF) analysis including the variables of 850 hPa wind, precipitation and sea level pressure]. The two leading modes of the EASM are presented in Fig. 2a, b. The first leading mode is characterized by the southwestern extension of the northwestern Pacific subtropical high, represented by an anticyclonic anomaly over the South China Sea and northwestern Pacific and an intense rainfall belt extending from the middle and lower reaches of the Yangtze River to Japan. The second leading mode is characterized by the eastward retreat of the northwestern Pacific subtropical high, corresponding to above-normal precipitation over northern China.

To gain better insight regarding the precipitation, the principal component of the first leading mode of East Asian precipitation is also used to compare the influence of these two factors, which we refer to as the PR index hereafter. Two leading summer rainfall patterns in East Asia are illustrated in Fig. 2c, d. The main rainfall belt is located along a

**Table 1** Comparison of the relative contributions of the IOBM and TP thermal heating to the EASM through correlation, partial correlation and standard multi-variable regression coefficients

|   | IOBM    | TP thermal heating |
|---|---------|--------------------|
| Correlation with the EASM index                   | 0.615** | 0.415*             |
| Partial correlation with the EASM index           | 0.589** | 0.361*             |
| Correlation with the PR index                     | 0.232   | 0.638**            |
| Partial correlation with the PR index             | 0.120   | 0.618**            |
| Standard regression coefficient on the EASM index | 0.550** | 0.292*             |
| Standard regression coefficient on the PR index   | 0.094   | 0.618**            |

Significance levels are indicated as 95 % (\*), and 99 % (\*\*)

route over the Sichuan Basin, Yangtze River, South Korea, and Japan. Despite the close correlation between the EASM index and PR index (correlation coefficient of 0.584, statistically significant at the 95 % confidence level), the EASM index better reflects the circulation pattern, while the PR index is a better representation of the precipitation pattern.

Station data are more credible than reanalysis data over the TP. However, regular surface station observations over the TP are distributed mainly in its central and eastern parts. In addition, station records of radiation are rare, and thus satellite radiation data are needed to obtain the total atmospheric heat source over the TP. Following Duan and Wu (2008), we first calculate the atmospheric heat source over the central and eastern TP using data from 71 meteorological stations and satellite radiation data, and then compare it with equivalent reanalysis data.

The atmospheric heat source is the sum of surface sensible heating, condensation heating, and radiation heating. Surface sensible heating (SH) is calculated by the four-times-daily surface temperature  $T_s$ , air temperature  $T_a$  (2 m) and surface wind  $V_0$  (10 m) based on the bulk formula

$$SH = \rho C_p C_{DH} V_0 (T_s - T_a)$$

where  $\rho$  is the air density,  $C_p = 1005 \text{ J kg}^{-1} \text{ K}^{-1}$  is the specific heat of dry air at constant pressure, and  $C_{DH}$  is the drag coefficient for heat. In the present study we take  $\rho = 0.8 \text{ kg m}^{-3}$  (Yeh and Gao 1979),  $C_{DH} = 4 \times 10^{-3}$  (Li and Yanai 1996) for the central-eastern TP, and  $C_{DH} = 4.75 \times 10^{-3}$  for the western TP (Li et al. 2000).

Condensation heating (LH) is estimated using precipitation (Pr):  $LH = Pr \times L_w \times \rho$ , where  $L_w = 2.5 \times 10^{-6} \text{ J kg}^{-1}$  is the condensation heating coefficient.

Radiation heating is calculated using the SRB data averaged over the TP. The column radiation heating (RC) is calculated by

$$RC = (S_{top}^\downarrow - S_{top}^\uparrow) - (S_{surf}^\downarrow - S_{surf}^\uparrow) - L_{top}^\uparrow - (L_{surf}^\downarrow - L_{surf}^\uparrow),$$

where the  $S$  and  $L$  quantities are the shortwave and long-wave radiation fluxes, respectively. The subscripts “top” and “surf” represent the fluxes at the top of the atmosphere and at the surface of the Earth, respectively. Upward arrows denote upward radiation fluxes, and vice versa.

Limited by the duration of the SRB data, the TP thermal heating, i.e. the sum of the SH, LH and RC over the TP, is available only from 1984 to 2007 based on station and satellite data. Therefore, the TP thermal heating is also calculated by the above method based on three reanalysis datasets, and they are interpolated onto the TP station data for evaluation. The correlation between the station data and the three sets of reanalysis data shows that JRA-55 presents the TP thermal heating the best (correlation coefficient of 0.834, as compared to 0.695 for ERA-Interim and 0.622 for NCEP/DOE). Thus, we select JRA-55 to obtain the TP thermal heating over the whole of the TP. In the following analysis, the TP thermal heating is calculated using the JRA-55 dataset for the time period of 1979–2007.

In addition, the index of the IOBM is the principal component of the first leading mode of summer tropical Indian Ocean (20°S–20°N, 40°–110°E) SST (Yang et al. 2007).

### 3 Data analysis

Table 1 summarizes the normal and partial correlation coefficients among the TP thermal forcing, IOBM index, EASM index, and PR index. The normal correlation between the summer TP thermal forcing and the EASM index is 0.415 (passing the 95 % significant test), while the correlation between the summer IOBM and EASM index is 0.615 (passing the 99 % significant test). It seems that, in terms of the circulation pattern, the TP thermal forcing has a relatively weaker relationship with the EASM index compared to that between the IOBM and EASM index. As for the correlation with the PR index, the results are totally different. The TP thermal heating correlates with the PR index quite well (0.638, passing the 99 % significant test), much higher than the correlation between the IOBM and PR index (0.232, not passing the significant test). Thus, in terms of the precipitation pattern, the TP thermal forcing seems to play a more important role than the IOBM in affecting the EASM. As documented by Wang et al. (2014), the mechanisms through which the TP affects the main rainfall belt of East Asia include the stationary wave excited by the TP thermal forcing, the warm advection from the TP, and the propagating synoptic disturbance from the TP.

To confirm this relationship is not changed by the interaction between the IOBM and TP thermal heating, partial correlations are calculated. The results show that the partial correlation between the IOBM and EASM index is still higher than that between the TP thermal heating and the

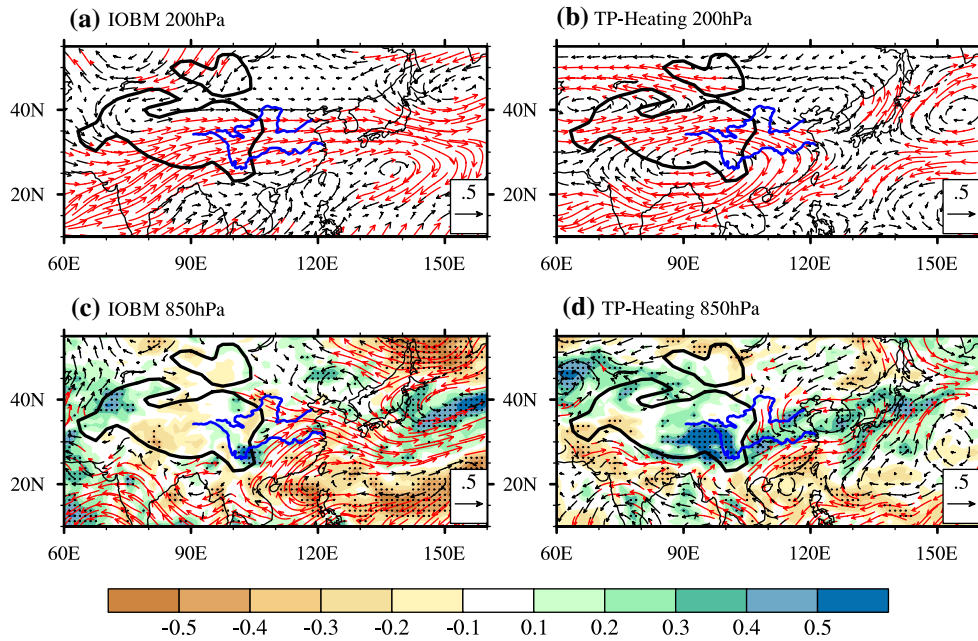


**Fig. 3** Partial correlations between winds/precipitation and the IOBM (**a, c**)/the TP thermal forcing (**b, d**) at 200 hPa (**a, b**) and 850 hPa (**c, d**) (shading: precipitation; vectors: wind; red vectors and

black dots indicate 90 % significance). The blue curves represent the Yangtze River and Yellow River from south to north, and the black bold curve denotes the area above 1,500 m

EASM index. For the PR index, the partial correlation with the TP thermal heating is higher than that with the IOBM. Note that the IOBM and TP thermal heating also show a weak positive correlation in interannual variability (correlation coefficient of 0.223, under the 90 % confidence level), suggesting that both the IOBM and TP thermal heating promote the relationship between the EASM and the other, making the partial correlations smaller than the normal correlations.

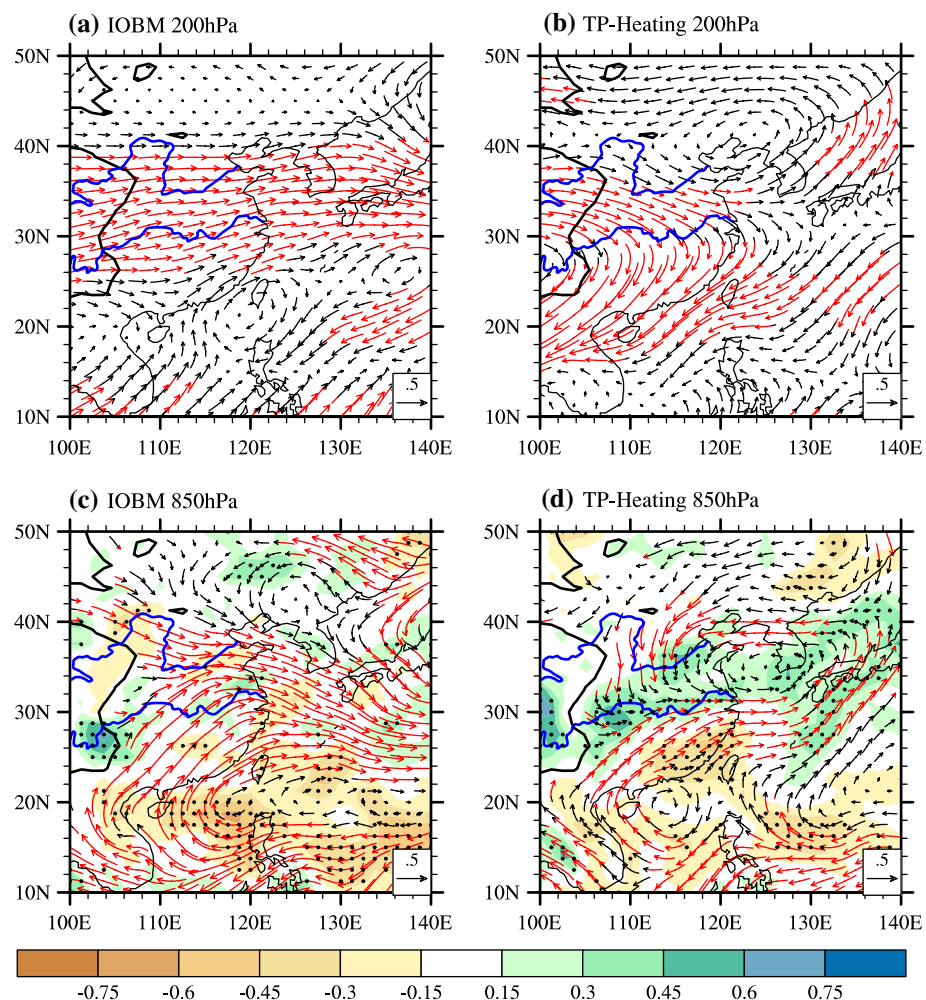
Another metric, multi-variable linear regression, is also used to compare the relative contributions of the IOBM and TP thermal heating. As seen from Table 1, when the IOBM and TP thermal heating are regressed onto the EASM index, it seems that the IOBM contributes more, but when they are regressed onto the PR index the TP thermal heating may play a more important role. This result is consistent with the results from the partial correlation analysis.

Maps of the partial correlations with circulation and precipitation can help us to further understand, in spatial distribution terms, the differences between the impacts of the IOBM and TP thermal heating on the EASM (Fig. 3). For circulation, the influence of the IOBM in the lower troposphere (850 hPa) is much stronger than that of the TP thermal heating. The positive phase of the IOBM (warm Indian Ocean SST) corresponds to an obvious anticyclonic anomaly over the northwestern Pacific, indicating an enhanced dominant mode of the EASM. This result is consistent with previous studies (Wu et al. 2009a; Xie

et al. 2009). In contrast, the TP thermal heating enhances both the southwesterly in southern China and northerly in northern China at lower levels, and this pattern is similar to the atmospheric response to the TP surface sensible heating (Wang et al. 2008a, 2014). At 200 hPa, both the IOBM and TP thermal forcing contribute to strengthen the South Asian high. The anticyclonic anomaly driven by the positive IOBM is located mainly on the eastern flank of the South Asian high, while the counterpart driven by the TP thermal heating is located mainly in the central part of the South Asian high, with a significantly enhanced easterly in its southern flank.

For precipitation, the impacts of the IOBM in East Asia are mainly in the southern part of the anticyclonic anomaly over the northwestern Pacific, while it has no significant effects in eastern China, the Korean Peninsula, and Japan. The TP thermal heating, however, has significant positive correlations with precipitation along the route over the Sichuan Basin, the middle and lower reaches of the Yangtze River, the Korean Peninsula, and Japan, representing a positive anomaly of the main rainfall belt of the EASM as shown in Fig. 2c. The corresponding lower-level circulation is characterized by an obvious convergence zone over the main rainfall belt between the anomalous northerly in northern China and the anomalous southwesterly in southern China. Clearly, such an anomalous precipitation pattern is analogous to the dominant mode of summer precipitation in East Asia (Fig. 2c), which is also consistent with the

**Fig. 4** Standard multi-variable regression coefficients of 200 hPa wind (**a, b**), 850 hPa wind (**c, d**) and precipitation (**c, d**) regressed on the IOBM (**a, c**)/TP thermal forcing (**b, d**) (shading: precipitation; vectors: wind; red vectors and black dots indicate 90 % significance). The blue curves represent the Yangtze River and Yellow River from south to north, and the black bold curve denotes the area above 1,500 m



results of Hsu and Liu (2003). Meanwhile, the TP thermal heating also has a significant negative correlation with the precipitation in southeastern China. Thus, in terms of the precipitation anomaly of the EASM, the TP thermal heating seems to play a more important role than the IOBM.

Figure 4 shows the spatial distribution of the standard multi-variable linear regression coefficients of wind and precipitation against the IOBM and TP thermal heating, separately, in which one can draw almost the same conclusion as that from the results based on the partial correlation. For the circulation at 200 hPa, the IOBM mainly affects the westerly anomaly between 30°N and 40°N, while the TP thermal heating mainly influences the anticyclonic anomaly over the TP. For the circulation at 850 hPa, the positive phase of the IOBM coincides with the strong northwestern Pacific anticyclonic anomaly. Although the positive TP thermal heating anomaly also correlates with the northwestern Pacific anticyclonic anomaly, its standard regression coefficients are smaller. In particular, it is also well correlated with the cyclonic anomaly over northeastern Asia to the north of the

anticyclonic anomaly, which provides the northerly anomaly and induces the resultant convergence zone along the main rainfall belt of the EASM in combination with the southerly anomaly accompanied by the northwestern Pacific anticyclonic anomaly.

For precipitation, the IOBM mainly contributes to the negative precipitation under the northwestern Pacific anticyclonic anomaly, and contributes little to the main rainfall belt of the EASM; while the TP thermal heating contributes substantially to the positive precipitation anomaly along the route over the Sichuan Basin, the middle and lower reaches of the Yangtze River, the Korean peninsula, and Japan. These results agree well with the partial correlation analysis above.

Generally, from the above comparisons using two statistical methods based on station observations and reanalysis data, the implication is that the IOBM can influence the dominant mode of the large-scale circulation of the EASM, while the TP thermal heating exerts a more direct and significant impact on the main rainfall belt associated with the EASM.

## 4 Numerical experiments

### 4.1 Experiment design

Simultaneous correlations based on data diagnosis cannot provide causal relationships among the TP thermal heating, IOBM and EASM. To confirm the data diagnosis results and compare the relative contributions from the IOBM and TP thermal heating on the EASM, a series of AGCM numerical experiments are conducted. The forcing fields employed in the IOBM and TP thermal heating experiments have almost the same magnitude compared to their respective natural variabilities. The natural inter-annual variability is quantified by the standard derivation ( $\sigma$ ) of the IOBM and TP thermal heating time series during 1979–2007. Here, both forcing fields are given the magnitude of  $2.5\sigma$ , and this magnitude of the anomaly is realistic. In some years, this  $2.5\sigma$  anomaly can be reached.

Anomalies with the magnitude of  $2.5\sigma$  of SST from the Hadley Center SST data are prescribed as the forcing field in the IOBM experiments. Since the variability of the tropical Indian Ocean ( $20^{\circ}\text{S}$ – $20^{\circ}\text{N}$ ,  $40^{\circ}$ – $110^{\circ}\text{E}$ ) SST represents the variability of the IOBM well (correlation coefficient of 0.983, passing the 99 % significant test), and the SST anomaly of the IOBM mode is almost uniform in the Indian Ocean basin, with a standard deviation of about 0.2 K, the 0.5 K SST anomalies are therefore added in the tropical Indian Ocean in the IOBM experiments. Besides, the TP thermal heating and SST anomalies over the Indian Ocean might influence each other to some degree. So, to remove this interaction effect, the IOBM experiments use the prescribed TP thermal heating from the control run over the TP region.

For the TP thermal heating experiments, considering the fact that the vertical profile of the diabatic heating anomaly is not always positive or negative from the bottom to the top of the atmosphere, we take the composite difference of the diabatic heating between the average of “strong years” and the average of “weak years” (defined as being  $0.7\sigma$  above or below the average) as the forcing, since the difference is nearly equal to  $2.5\sigma$  for the TP thermal heating (Fig. 5b, c).

The spatial distribution and vertical profile of the composite difference over the TP are shown in Fig. 5a. The main anomalies are concentrated over the central and eastern TP ( $85^{\circ}$ – $105^{\circ}\text{E}$ ,  $25^{\circ}$ – $35^{\circ}\text{N}$ ), and the anomalies over the western TP in summer are relatively weaker. Condensation heating dominates the total atmospheric heating in summer (Yeh and Gao 1979; Yanai and Wu 2006). Therefore, to simplify the experiment, only the condensation heating anomaly is considered in the TP thermal heating experiments. Note that the climate mean precipitation amount decreases northward over the central and eastern TP, and

the average heating anomaly to the north of  $35^{\circ}\text{N}$  is only 1/4 of the heating anomaly in the southern part; hence, we use 1/4 of the heating anomaly to the north of  $35^{\circ}\text{N}$  compared to the southern part (Fig. 5a). Since the added condensation heating is much smaller than the surrounding condensation heating, the numerical artifacts due to the discontinuous boundary can be neglected.

Four sets of AGCM experiments are conducted (Table 2). The first is the control run (CONTROL), in which the climate mean monthly SST and sea ice with seasonal evolution is prescribed, and the diabatic heating output is stored. The second is the TP thermal heating run, named TP HEATING, in which an anomaly of condensation heating of nearly  $2.5\sigma$  over the central and eastern TP is added in summer (JJA), as shown in Fig. 6. The third is the IOBM run with the prescribed TP thermal heating, named IOBM\_TPCTRL, where 0.5 K SST anomalies are added in the tropical Indian Ocean (the anomalies are uniform within  $(15^{\circ}\text{S}$ – $15^{\circ}\text{N}$ ,  $50^{\circ}$ – $100^{\circ}\text{E}$ ), and then gradually taper towards 0 until reaching  $20^{\circ}\text{S}$ ,  $20^{\circ}\text{N}$ ,  $40^{\circ}\text{E}$ , and  $110^{\circ}\text{E}$ ), as shown in Fig. 7. The fourth experiment is also an IOBM run, named IOBM\_TPFREE, where the TP thermal heating is not prescribed, to explore the impacts of the IOBM on the TP thermal heating (discussed in Sect. 5). The three sensitivity experiments comprise 20 ensembles with different initial ensembles, and both positive and negative anomaly experiments are conducted.

### 4.2 Experiments results

The dominant low-level circulation components over the Asian summer monsoon regions are the Somali jet, the southerly in southern China, and the northwestern Pacific subtropical high, accompanied by precipitation of above  $5 \text{ mm day}^{-1}$  in most parts of East Asia (Fig. 8a). All these features can be successfully reproduced by FAMIL, although the southerly over eastern China is overestimated by about  $2 \text{ m s}^{-1}$ , and the rainfall amount over the region east of  $120^{\circ}\text{E}$  in East Asia is underestimated by about  $2 \text{ mm day}^{-1}$  (Fig. 8b). Thus, we have confidence in conducting the sensitivity experiments. Note that all the experiment results presented are the differences between the positive and negative anomaly experiments.

The effects of the IOBM on the EASM without considering its influence on condensation heating over the TP are shown in the left panels of Fig. 9, and the influences of the TP thermal heating are presented in the right panels. It can be seen that the warm Indian Ocean SST (i.e. the positive phase of the IOBM) excites a Gill-type pattern circulation response, characterized by a westerly anomaly in the upper troposphere and a strong Kelvin wave-type easterly anomaly in the lower troposphere over the tropics. According to Wu et al. (2009a, b, c) and Xie et al. (2009), Kelvin

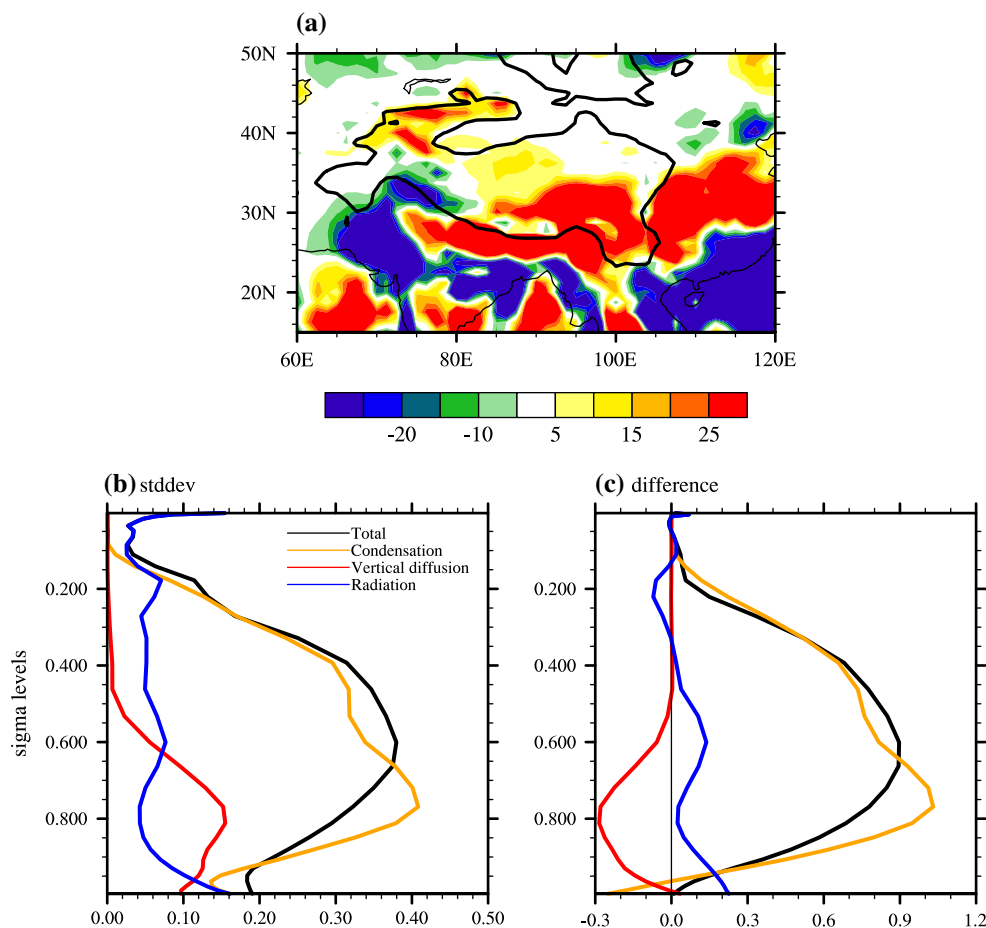


**Fig. 5** Difference of total diabatic heating between “strong years” and “weak years” of the TP thermal forcing (a) (units:  $\text{W m}^{-2}$ ). The vertical profile of the standard deviation of the diabatic heating (including total heating, condensation heating, vertical diffusion heating and radiation heating) over the central and eastern TP ( $25^{\circ}\text{--}35^{\circ}\text{N}$ ,

$85^{\circ}\text{--}105^{\circ}\text{E}$ ) (b) (units:  $\text{K day}^{-1}$ ). The difference of the vertical profile of the diabatic heating between “strong years” and “weak years” of the TP thermal forcing over the central and eastern TP (c) (units:  $\text{K day}^{-1}$ )

wave-type easterly anomalies with anticyclone shear over the northwestern Pacific lead to divergence in the planetary boundary layer, suppressing convective activity in this area and then generating an anticyclonic anomaly and weak precipitation over the northwestern Pacific. By the similar mechanism, an anticyclonic anomaly also appears over the Bay of Bengal in both the middle and low levels. The anticyclonic anomaly over the northwestern Pacific is one of the main components of the EASM’s circulation system (Fig. 2a), which is consistent with the analysis results based on observations. We note that the closed anticyclone over the northwestern Pacific does not stretch eastward to  $150^{\circ}\text{E}$  as in previous studies. This may be related to the weakness of the western North Pacific monsoon trough in FAMIL, whose establishment favors the impacts of the IOBM on the anticyclone anomaly over the northwestern Pacific (Wu et al. 2010). As for the precipitation anomalies in the IOBM experiments, significant negative precipitation anomalies

under the anticyclones over both the tropical Indian Ocean and the northwestern Pacific are the main characteristics. In the subtropics, however, significant positive precipitation anomalies appear only over the south and east edges of the TP, while significant negative precipitation anomalies exist over and to the east of Japan.

Results from TP HEATING indicate that strong diabatic heating over the TP will substantially enhance the South Asian high situated above. Near the surface of the TP (500 hPa), the corresponding circulation response is an intensified cyclonic circulation anomaly, indicating a baroclinic structure in the vertical direction. To the northeast of the TP, the cyclonic anomaly exists in almost the entire troposphere from 850 to 200 hPa, showing a barotropic structure, which does not appear in the IOBM experimental results. This cyclonic anomaly could be viewed as part of a wave train originating from the TP (Wang et al. 2008a, 2014). This Rossby wave train, which can be seen clearly

**Table 2** Design of the AGCM experiments

| Experiment  | Design  |
|-------------|---|
| CONTROL     | Prescribed global climatological SST/sea ice  |
| TP HEATING  |   |
| Positive    | Add $2.5\sigma$ condensation heating profile in the central-eastern TP                            |
| Negative    | Remove $2.5\sigma$ condensation heating profile in the central-eastern TP                         |
| IOBM_TPCTRL |   |
| Positive    | Add 0.5 K SST in the tropical Indian Ocean, with prescribed TP condensation heating in CONTROL    |
| Negative    | Remove 0.5 K SST in the tropical Indian Ocean, with prescribed TP condensation heating in CONTROL |
| IOBM_TPFREE |   |
| Positive    | Add 0.5 K SST in the tropical Indian Ocean  |
| Negative    | Remove 0.5 K SST in the tropical Indian Ocean   |

in Fig. 9b, starts from the anticyclone anomaly over the TP, propagates northeastward to form the barotropic cyclone anomaly over northeastern China, and then moves eastward, forming the anticyclone anomaly to the east of Japan. Meanwhile, the circulation response to the southeast of the TP, i.e. southern China, is a similar anticyclonic anomaly as in the IOBM experimental results, and the magnitude of southwesterly anomalies over southern China in TP HEATING is comparable with that in the IOBM experiments. Subsequently, a convergence belt between cold and dry airflow from higher latitudes, and warm and wet airflow from the tropical oceans, occurs in the subtropics (about  $30^{\circ}$ – $35^{\circ}$ N) over eastern China in the lower troposphere, coinciding with the main rainfall belt of the EASM as introduced before, and hence enhances it significantly. This significant positive precipitation anomaly over the main rainfall belt does not appear in the IOBM experiments.

Overall, the northerly anomaly induced by the cyclonic response over northern China is necessary to modulate the intensity and the location of the convergence zone and the main rainfall belt of the EASM. This can explain why a significant precipitation anomaly appears only in TP HEATING and not in the IOBM experiments.

## 5 Impacts of the IOBM on the TP thermal heating

In Sect. 3 it is mentioned that the IOBM index is positively correlated with the TP thermal heating index, although the correlation between them is not statistically significant. This implies the possibility that the Indian Ocean SST could influence the TP thermal heating. Since the TP thermal heating in summer is dominated mainly by the southeastern TP precipitation, the IOBM may affect the TP

thermal heating through influencing the precipitation over the southeastern TP. Thus, in this section we mainly discuss the possible impacts of the IOBM on the TP precipitation.

The spatial distribution of the correlation between the IOBM index and the precipitation (10 m wind) over the TP (Fig. 10) indicates that the positive phase of the IOBM corresponds to enhanced precipitation over the southeastern TP and less rainfall over the southwestern TP. During positive IOBM phases, at the surface, a southwesterly anomaly exists from the northern Bay of Bengal to the southeastern TP, while at high levels anticyclonic curves lie over the southeastern TP. Also, there are northerly anomalies north of the enhanced rainfall area. The southwesterly anomaly brings a substantial amount of water vapor from the tropical oceans, such as from the Bay of Bengal, and converges with the northerly anomaly. Meanwhile, this process is accompanied by a significant westerly anomaly in the upper troposphere (200 hPa) over most parts of TP and an anticyclonic circulation anomaly over the southeastern corner. Therefore, convergence in the lower layers and divergence in the upper layers brings about the positive precipitation anomaly over the southeastern TP.

To elucidate the causal relationship between the IOBM and the TP precipitation, and further confirm the above results from data analysis, numerical experiments are required. Accordingly, the results of the IOBM\_TPFREE experiment (Fig. 11) are used to explore whether or not warm Indian Ocean SST could cause enhanced precipitation over the southeastern TP. The indication is that warm Indian Ocean SST (i.e. the positive phase of the IOBM) does indeed cause enhanced rainfall over the southeastern TP, as well as less rainfall over the southwestern TP. In addition, the circulation pattern is similar to that established via the data analysis results. At 200 hPa, an anticyclonic anomaly appears over the southeastern TP. Near the surface, the warm Indian Ocean SST excites not only an anticyclonic anomaly over the northwestern Pacific, but also an anticyclonic anomaly over the Bay of Bengal. On the northwestern flank of the anticyclonic anomaly over the Bay of Bengal, the southwesterly anomaly converges with the northerly anomaly in the southeastern TP and facilitates abundant precipitation over the region. Feng and Zhou (2012) also noted the importance of this anticyclonic anomaly over the Bay of Bengal, illustrating that it mainly controls the interannual variability of summer TP precipitation. Therefore, a positive IOBM may intensify the atmospheric heat source over the TP to a certain degree.

## 6 Conclusions and discussion

The present study compares the impacts of two different factors (the IOBM, an ocean factor, and TP thermal heating,

**Fig. 6** Horizontal (a) [red coloring represents the vertical profile in (b); yellow represents 1/4 times the vertical profile in (b); and the contour is the 1,500 m surface height] and vertical (b) (units:  $\text{K day}^{-1}$ ) distribution of the condensation heating added into TP HEATING (positive runs)

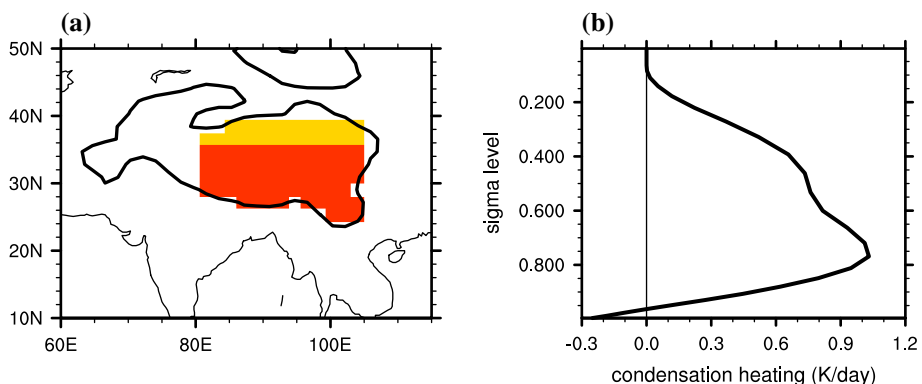


**Fig. 7** SST anomalies (a positive runs; b negative runs) added into the IOBM\_TPCTRL and IOBM\_TPFREE experiments (units: K). The anomalies are uniform within ( $15^{\circ}\text{S}$ – $15^{\circ}\text{N}$ ,  $50^{\circ}$ – $100^{\circ}\text{E}$ ), and then gradually taper towards 0 until reaching  $20^{\circ}\text{S}$ ,  $20^{\circ}\text{N}$ ,  $40^{\circ}\text{E}$ , and  $110^{\circ}\text{E}$

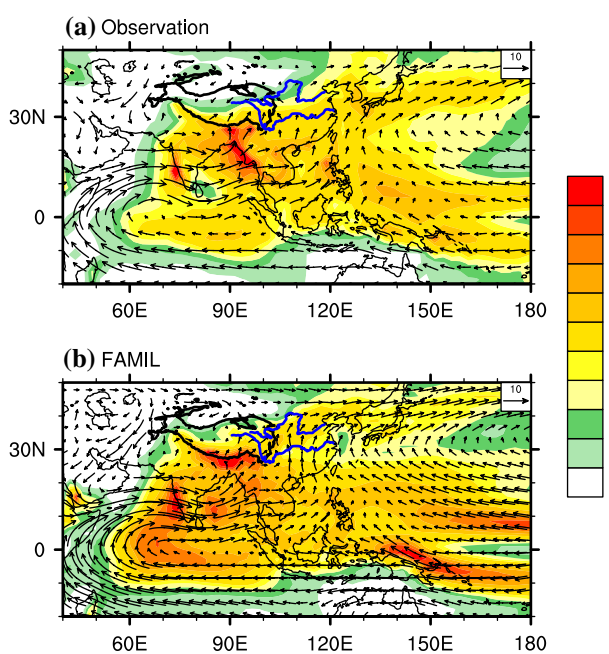
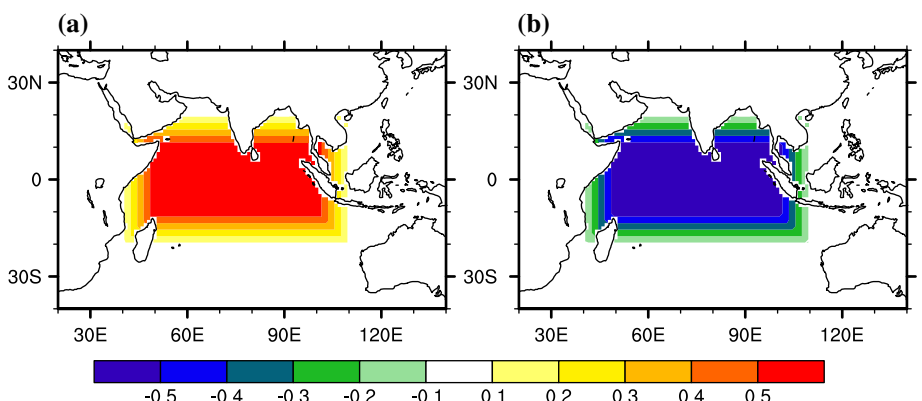


**Fig. 8** Climate mean 850 hPa wind and precipitation from observation (a) and FAMIL control run (b) (units of wind:  $\text{m s}^{-1}$ ; units of precipitation:  $\text{mm day}^{-1}$ ; blue curves represent the Yangtze River and Yellow River from south to north, and the black bold curve denotes the area above 1,500 m)

a land factor) on the interannual variability of the EASM in terms of large-scale circulation and precipitation. The relative contribution of the IOBM and TP thermal heating are compared by both data analysis and numerical experiments. The data analysis shows that the IOBM may impact the large-scale circulation of the EASM more significantly, especially with respect to the northwestern Pacific subtropical high in the middle and lower troposphere, while the TP thermal heating might play a more important role in affecting the main rainfall belt along the route over the Sichuan Basin, the middle-to-lower reaches of the Yangtze River, the Korean Peninsula, and Japan.

The experimental results from the AGCM further confirm that the IOBM is the main driver of the anticyclonic anomaly over the northwestern Pacific in the lower troposphere, while the TP thermal heating primarily excites the southwesterly in the lower layers and strong anticyclonic anomaly over and around the TP in the upper troposphere. Although the southwesterly anomaly over southern China driven by the IOBM is comparable with that in the TP thermal heating experiment, a significant northerly anomaly over northern China can be detected only in the TP thermal heating experiment, which converges with the southwesterly anomaly from southern China in the subtropics (roughly between  $30^{\circ}\text{N}$  and  $35^{\circ}\text{N}$ ). As a result, the main rainfall belt of the EASM is enhanced. In fact, this

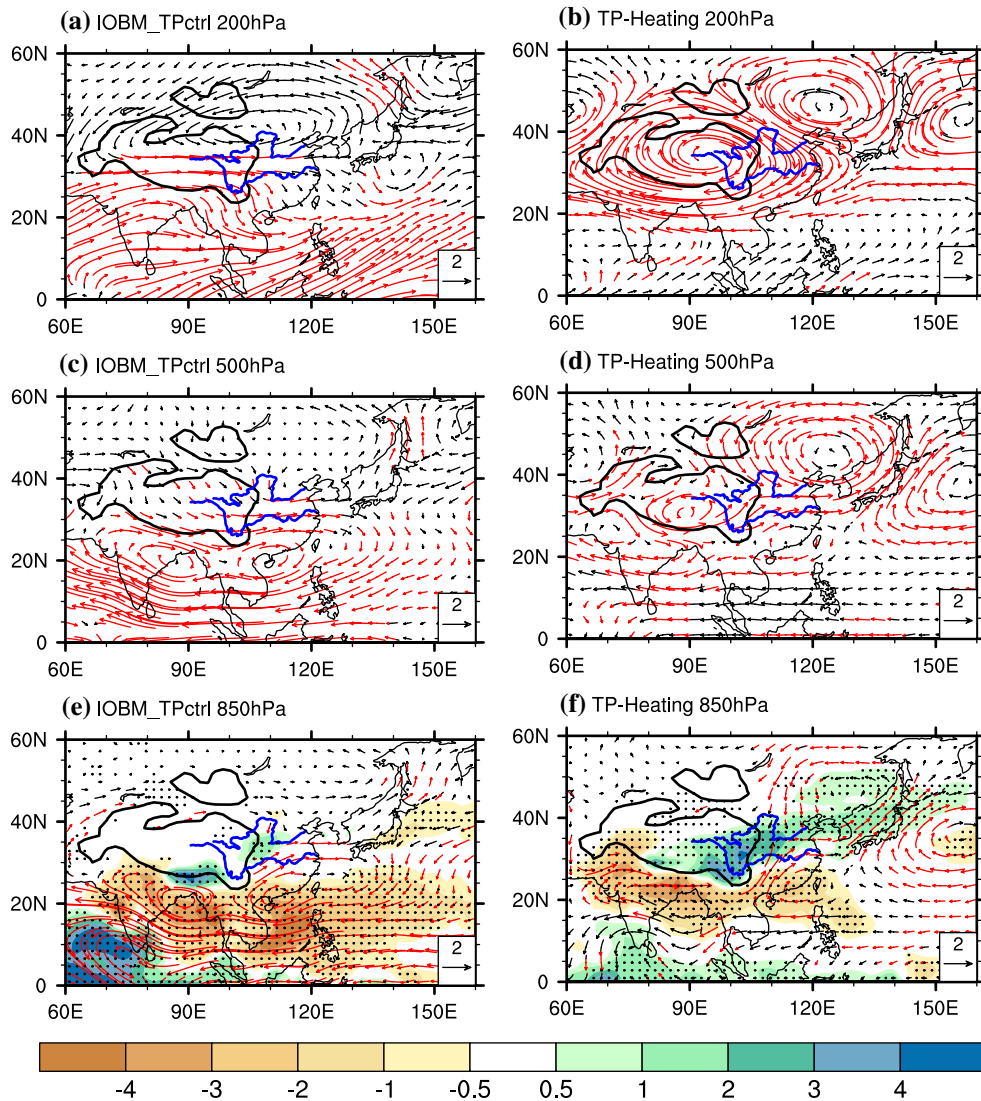


**Fig. 9** Difference fields of wind at 200 hPa (**a**, **b**), 500 hPa (**c**, **d**), 850 hPa (**e**, **f**) (vectors, units:  $\text{m s}^{-1}$ ; red vectors indicate 90 % significance) and precipitation (shading, units:  $\text{mm day}^{-1}$ ; black dots indicate 90 % significance) between positive and negative experimental

results in IOBM\_TPCTRL (**a**, **c**, **e**) and TP HEATING (**b**, **d**, **f**). Blue curves represent the Yangtze River and Yellow River from south to north, and the black bold curves denote the area above 1,500 m

northerly anomaly is a part of a wave train generated by the TP thermal heating with a near barotropic structure. In contrast, the IOBM cannot directly produce significant circulation anomalies over the mid and high latitudes, and its main contribution in terms of precipitation is along the south flank of the anticyclonic anomaly over the northwestern Pacific. In addition, the impacts of the IOBM on the TP thermal heating are further investigated. Both the data diagnosis and the numerical experiment results indicate that warm Indian Ocean SST causes enhanced precipitation over the southeastern TP, leading to the increased TP thermal heating over the region.

TP thermal heating playing a more important role in East Asian summer precipitation implies that if we focus on

the rainfall of the EASM, we should examine and improve the capabilities of models in simulating the variability of the TP thermal heating and reproducing the responses stimulated by the TP thermal heating. In contrast, model skill in reproducing the IOBM–EASM teleconnection has long been a concern. Song and Zhou (2014) indicated that models with high skill in reproducing the interannual variability are better at simulating the ENSO–Indian Ocean–western Pacific anticyclone teleconnection.

In this study we compare the contribution of the IOBM and TP thermal heating during the whole summer season from June to August. Previous studies have pointed out that the characteristics of the circulation and precipitation patterns of the EASM in individual months and the

**Fig. 10** Correlations between the IOBM index and winds at 200 hPa (a) and 10 m above the surface (b) (vectors; red vectors indicate 90 % significance) and precipitation (b) (shading; black dots indicate 90 % significance). The blue curves represent the Yangtze River and Yellow River from south to north, and the black bold curves denote area the above 1,500 m

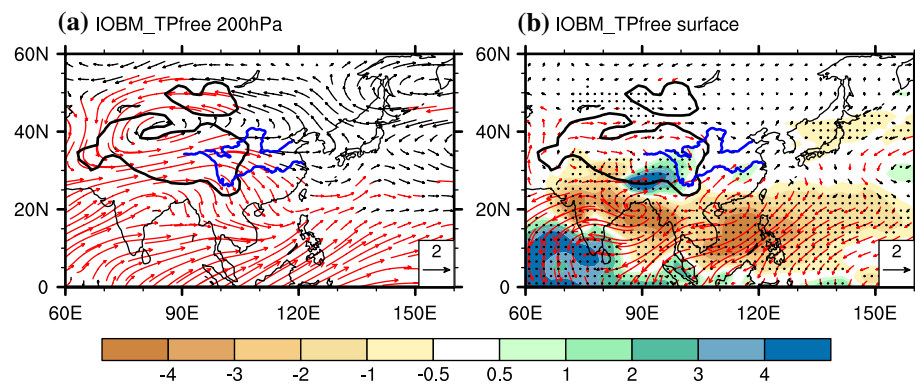
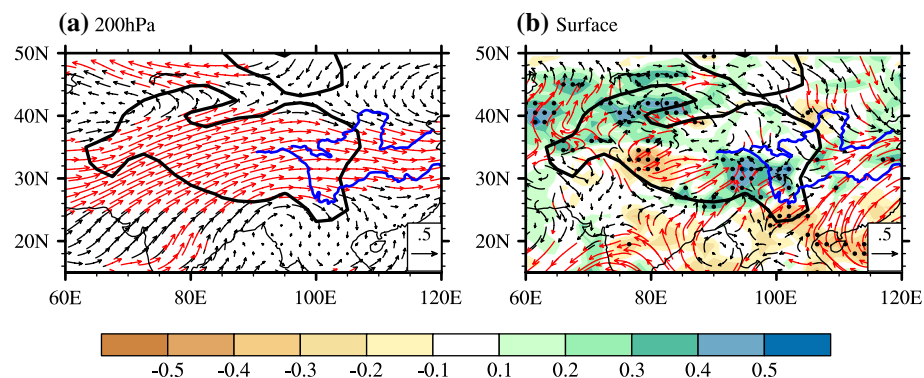


**Fig. 11** Difference fields of winds at 200 hPa (a) and 10 m above the surface (b) (vectors, units:  $\text{m s}^{-1}$ ; red vectors indicate 90 % significance) and precipitation (b) (shading, units:  $\text{mm day}^{-1}$ ; black dots indicate 90 % significance) between positive and negative experiments in IOBM\_TPfree. Blue curves represent the Yangtze River and Yellow River from south to north, and the black bold curves denote area the above 1,500 m

mental results in IOBM\_TPfree. Blue curves represent the Yangtze River and Yellow River from south to north, and the black bold curves denote area the above 1,500 m

mechanisms for their variability are different (Wang et al. 2009a). For example, the relative contributions of the Indian Ocean and northwestern Pacific SSTs to the northwestern Pacific anticyclonic anomalies show some differences in June, July and August (Wu et al. 2010; Xiang et al. 2013). Thus, it is possible that our conclusion based on the months of June–August may be somewhat different if each specific month is examined.

Our study has also touched upon the possible impacts of the IOBM on the TP thermal heating. The variation of the TP thermal heating due to the IOBM may also influence the variability of the EASM. There are some clues in Fig. 11. The thermal heating anomaly over the south flank of the TP induced by the IOBM does not generate the cyclonic anomaly over northeastern Asia as expected, which seems to indicate that the proportion of the TP thermal heating variability caused by the IOBM cannot significantly influence the EASM. The reason might be that the area of the thermal heating anomaly is smaller and confined to the south flank of the TP, and this thermal heating anomaly is not stationary during the whole boreal summer. Thus, from our study, the impacts of the IOBM and

the TP thermal heating are largely separated. These “one-on-one” (i.e., IOBM  $\rightarrow$  EASM and TP  $\rightarrow$  EASM) processes are more dominant than the “chain reaction” (i.e., IOBM  $\rightarrow$  TP  $\rightarrow$  EASM) processes, but this needs further detailed investigations. On the other hand, the TP thermal heating may in turn influence SST. Zhou et al. (2009) indicated that TP thermal heating could drive a teleconnection pattern like the Asian–Pacific Oscillation (APO), affecting circulation and climate in North America, Europe and the southern Indian Ocean. Nan et al. (2009) demonstrated that air temperature over the TP could impact the tropical eastern Pacific SST via the APO, and hence establish the relationship between the TP thermal heating and ENSO. We notice that the previous winter ENSO is well correlated with the IOBM. Therefore, the interaction between the TP thermal heating and the IOBM and the impacts of their interaction on the EASM will be investigated in future work by using an air–sea coupled general circulation model.

Finally, to better understand the mechanism involved, our study uses only two factors impacting on the EASM in the same season. In future work, factors impacting on the

EASM in the leading seasons need to be considered to provide useful insights for the prediction of EASM interannual variability. As illustrated in Fig. 1, ENSO in the previous winter bears a close leading correlation with the EASM, as does the IOD in the previous autumn. Land and snow cover/depth signals over Eurasia in the previous winter and spring will be considered by our group in future work.

**Acknowledgments** We thank Prof. Yimin Liu for providing constructive suggestions regarding experimental design, and thank two anonymous reviewers for their insightful comments. This work was supported jointly by the National Natural Science Foundation of China (Grant Nos. 91337216 and 41175070) and the Special Fund for Public Welfare Industry (meteorology) administered by the Chinese Ministry of Finance and the Ministry of Science and Technology (Grant No. GYHY201406001).

## References

- Adler RF, Huffman GJ, Chang A et al (2003) The version-2 global precipitation climatology project (GPCP) monthly precipitation analysis (1979–present). *J Hydrometeorol* 4:1147–1167
- Chang CP, Zhang Y, Li T (2000) Interannual and interdecadal variations of the East Asian summer monsoon and tropical Pacific SSTs. Part I: roles of the subtropical ridge. *J Clim* 13:4310–4325
- Clough SA, Shephard MW, Mlawer EJ, Delamere JS, Iacono MJ, Cady-Pereira K, Boukabara S, Brown PD (2005) Atmospheric radiative transfer modeling: a summary of the AER codes. *J Quant Spectrosc Radiat Transf* 91:233–244
- Dee DP, Uppala SM, Simmons AJ et al (2011) The ERA-Interim reanalysis: configuration and performance of the data assimilation system. *Q J R Meteorol Soc* 137:553–597
- Ding Y, Chan JC (2005) The East Asian summer monsoon: an overview. *Meteorol Atmos Phys* 89:117–142
- Duan AM, Wu GX (2005) Role of the Tibetan Plateau thermal forcing in the summer climate patterns over subtropical Asia. *Clim Dyn* 24:793–807
- Duan AM, Wu GX (2008) Weakening trend in the atmospheric heat source over the Tibetan plateau during recent decades. Part I: observations. *J Clim* 21:3149–3164
- Duan AM, Wang MR, Lei YH, Cui YF (2013) Trends in summer rainfall over China associated with the Tibetan Plateau sensible heat source during 1980–2008. *J Clim* 26:261–275
- Ebita A, Kobayashi S, Ota Y et al (2011) The Japanese 55-year reanalysis “JRA-55”: an interim report. *SOLA* 7:149–152
- Edwards JM, Slingo A (1996) Studies with a flexible new radiation code. 1. Choosing a configuration for a large-scale model. *Q J R Meteorol Soc* 122:689–719
- Feng L, Zhou T (2012) Water vapor transport for summer precipitation over the Tibetan Plateau: multidata set analysis. *J Geophys Res* 117:D20114. doi:[10.1029/2011JD017012](https://doi.org/10.1029/2011JD017012)
- Fu CB, Teng XL (1988) Summer climate anomalies of China in association with ENSO phenomenon. *Sci Atmos Sin* special issue for 60th anniversary of IAP, pp 125–137
- Gong DY, Ho CH (2003) Arctic oscillation signals in the East Asian summer monsoon. *J Geophys Res* 108(D2):4066. doi:[10.1029/2002JD002193](https://doi.org/10.1029/2002JD002193)
- Gong Y, Ji L (1998a) The numerical experiment of the medium-range change of the subtropical high I: the influence of the heat source over Tibetan Plateau. *J Trop Meteorol* 14(2):106–112
- Gong Y, Ji L (1998b) The numerical experiment of the medium-range change of the subtropical high II: the influence of the heat source over tropical western Pacific. *J Trop Meteorol* 14(3):201–207
- Gong DY, Yang J, Kim SJ, Gao Y, Guo D, Zhou T, Hu M (2011) Spring Arctic oscillation-East Asian summer monsoon connection through circulation changes over the western North Pacific. *Clim Dyn* 37:2199–2216
- Harris LM, Lin SJ (2014) Global-to-regional nested grid climate simulations in the GFDL high resolution atmospheric model. *J Clim* 27(13):4890–4910
- Holtslag AAM, Boville BA (1993) Local versus nonlocal boundary-layer diffusion in a Global Climate Model. *J Clim* 6:1825–1842
- Hsu HH, Liu X (2003) Relationship between the Tibetan Plateau heating and East Asian summer monsoon rainfall. *Geophys Res Lett* 30(20):2066. doi:[10.1029/2003GL017909](https://doi.org/10.1029/2003GL017909)
- Huang R (1985) The influence of the heat source anomaly over Tibetan Plateau on the northern hemispheric circulation. *Acta Meteorol Sin* 43(2):208–220
- Huang SS, Yang XQ, Jiang QR, Tang MM, Wang ZM, Xie Q, Zhu YC (1995) The effects of the polar sea ice on climate. *J Meteorol Sci* 15(4):46–56 (in Chinese)
- Jian M, Luo H, Qiao Y (2004) On the relationships between the summer rainfall in China and the atmospheric heat sources over the Eastern Tibetan Plateau and the Western Pacific warm pool. *J Tropical Meteorol* 20(4):355–364
- Kanamitsu M, Ebisuzaki W, Woollen J, Yang S, Hnilo JJ, Fiorino M, Potter GL (2002) NCEP–DOE AMIP-II reanalysis (R-2). *Bull Am Meteorol Soc* 83:1631–1643
- Li CF, Yanai M (1996) The onset and interannual variability of the Asian summer monsoon in relation to land–sea thermal contrast. *J Clim* 9:358–375
- Li G, Duan T, Gong Y (2000) The bulk transfer coefficients and surface fluxes on the western Tibetan Plateau. *Chin Sci Bull* 45:1221–1226
- Liu YM, Wu GX, Ren RC (2004) Relationship between the subtropical anticyclone and diabatic heating. *J Clim* 17:682–698
- Luo H, Chen R (1995) The impact of the anomalous heat sources over the Eastern Tibetan Plateau on the circulation over East Asia in summer half year. *Sci Meteorol Sin* 15(4):94–102
- Nan S, Li J (2003) The relationship between the summer precipitation in the Yangtze River valley and the boreal spring Southern Hemisphere annular mode. *Geophys Res Lett* 30(24):2266. doi:[10.1029/2003GL018381](https://doi.org/10.1029/2003GL018381)
- Nan SL, Li JP, Yuan XJ, Zhao P (2009) Boreal spring Southern Hemisphere annular mode, Indian Ocean sea surface temperature, and East Asian summer monsoon. *J Geophys Res* 114:D02103. doi:[10.1029/2008JD010045](https://doi.org/10.1029/2008JD010045)
- Nordeng TE (1994) Extended versions of the convective parameterization scheme at ECMWF and their impact on the mean and transient activity of the model in the tropics. Research Department Technical Memorandum No. 206, ECMWF, Shinfield Park, Reading, UK
- Palmer TN, Shutt GJ, Swinbank R (1986) Alleviation of a systematic westerly bias in general-circulation and numerical weather prediction models through an orographic gravity-wave drag parameterization. *Q J R Meteorol Soc* 112:1001–1039
- Rayner NA, Parker DE, Horton EB, Folland CK, Alexander LV, Rowell DP, Kent EC, Kaplan A (2003) Global analyses of sea surface temperature, sea ice, and night marine air temperature since the late nineteenth century. *J Geophys Res* 108(D14):4407. doi:[10.1029/2002JD002670](https://doi.org/10.1029/2002JD002670)
- Saji NH, Yamagata T (2003) Possible impacts of Indian Ocean dipole mode events on global climate. *Clim Res* 25(2):151–169
- Song F, Zhou T (2014) Interannual variability of East Asian summer monsoon Simulated by CMIP3 and CMIP5 AGCMs: skill dependence on Indian Ocean–Western Pacific anticyclone teleconnection. *J Clim* 27:1679–1697
- Sun Z (2011) Improving transmission calculations for the Edwards–Slingo radiation scheme using a correlated-k distribution method. *Q J R Meteorol Soc* 137:2138–2148. doi:[10.1002/qj.880](https://doi.org/10.1002/qj.880)

- Tiedtke M (1989) A comprehensive mass flux scheme for cumulus parameterization in large-scale models. *Mon Weather Rev* 117:1779–1800
- Wang B, Wu RG, Fu XH (2000) Pacific-East Asian teleconnection: How does ENSO affect East Asian climate? *J Clim* 13:1517–1536
- Wang B, Bao Q, Hoskins B, Wu GX, Liu YM (2008a) Tibetan plateau warming and precipitation changes in East Asia. *Geophys Res Lett* 35:L14702. doi:[10.1029/2008GL034330](https://doi.org/10.1029/2008GL034330)
- Wang B, Wu ZW, Li JP, Liu J, Chang CP, Ding YH, Wu GX (2008b) How to measure the strength of the East Asian summer monsoon. *J Clim* 21:4449–4463
- Wang B, Liu J, Yang J, Zhou T, Wu Z (2009a) Distinct principal modes of early and late summer rainfall anomalies in East Asia. *J Clim* 22:3864–3875
- Wang B, Lee JY, Kang IS et al (2009b) Advance and prospectus of seasonal prediction: assessment of the APCC/CliPAS 14-model ensemble retrospective seasonal prediction (1980–2004). *Clim Dyn* 33:93–117
- Wang B, Xiang B, Lee JY (2013) Subtropical high predictability establishes a promising way for monsoon and tropical storm predictions. *Proc Natl Acad Sci* 110:2718–2722
- Wang Z, Duan A, Wu G (2014) Time-lagged impact of spring sensible heat over the Tibetan Plateau on the summer rainfall anomaly in East China: case studies using the WRF model. *Clim Dyn* 42:2885–2898
- Weng H, Ashok K, Behera S, Rao S, Yamagata T (2007) Impacts of recent El Niño Modoki on dry/wet conditions in the Pacific rim during boreal summer. *Clim Dyn* 29:113–129
- Wu RG, Kirtman BP (2007) Observed relationship of spring and summer East Asian rainfall with winter and spring Eurasian snow. *J Clim* 20:1285–1304
- Wu TW, Qian ZA (2003) The relation between the Tibetan winter snow and the Asian summer monsoon and rainfall: an observational investigation. *J Clim* 16:2038–2051
- Wu G, Liu H, Zhao Y, Li W (1996) A nine-layer atmospheric general circulation model and its performance. *Adv Atmos Sci* 13(1):1–18
- Wu B, Zhou TJ, Li T (2009a) Seasonally evolving dominant interannual variability modes of East Asian climate. *J Clim* 22:2992–3005
- Wu BY, Zhang RH, Wang B, D'Arrigo R (2009b) On the association between spring Arctic sea ice concentration and Chinese summer rainfall. *Geophys Res Lett* 36:L09501. doi:[10.1029/2009GL037299](https://doi.org/10.1029/2009GL037299)
- Wu Z, Wang B, Li J, Jin FF (2009c) An empirical seasonal prediction model of the East Asian summer monsoon using ENSO and NAO. *J Geophys Res* 114:D18120
- Wu B, Li T, Zhou TJ (2010) Relative contributions of the Indian Ocean and Local SST anomalies to the maintenance of the Western North Pacific anomalous anticyclone during the El Niño decaying summer. *J Clim* 23:2974–2986
- Wu GX, Liu YM, He B, Bao Q, Duan AM, Jin FF (2012) Thermal controls on the Asian summer monsoon. *Sci Rep* 2:404. doi:[10.1038/srep00404](https://doi.org/10.1038/srep00404)
- Xiang B, Wang B, Yu W, Xu S (2013) How can anomalous western North Pacific Subtropical High intensify in late summer? *Geophys Res Lett* 40:2349–2354
- Xie SP, Hu KM, Hafner J, Tokinaga H, Du Y, Huang G, Sampe T (2009) Indian ocean capacitor effect on Indo-Western Pacific Climate during the summer following El Niño. *J Clim* 22:730–747
- Yanai M, Wu GX (2006) Effects of the Tibetan Plateau. In: Wang B (ed) *The Asian monsoon*. Springer Praxis, Chichester, pp 513–549
- Yang S, Lau KM (1998) Influences of sea surface temperature and ground wetness on Asian summer monsoon. *J Clim* 11:3230–3246
- Yang S, Lau KM (2006) Interannual variability of the Asian monsoon. In: Wang B (ed) *The Asian monsoon*. Springer Praxis, Chichester, pp 259–293
- Yang JL, Liu QY, Xie SP, Liu ZY, Wu LX (2007) Impact of the Indian Ocean SST basin mode on the Asian summer monsoon. *Geophys Res Lett* 34:L02708. doi:[10.1029/2006GL028571](https://doi.org/10.1029/2006GL028571)
- Yasutomi N, Hamada A, Yatagai A (2011) Development of a long-term daily gridded temperature dataset and its application to rain/snow discrimination of daily precipitation. *Glob Environ Res* 15(2):165–172
- Ye B, Yang D, Ding Y, Han T, Koike T (2004) A bias-corrected precipitation climatology for China. *J Hydrometeorol* 5:1147–1160
- Yeh TC, Gao YX (1979) *Meteorology of the Qinghai-Xizang (Tibet) Plateau*. Science Press, Beijing
- Yu HY, Bao Q, Zhou LJ (2014) Sensitivity of precipitation in aquaplanet experiments with an AGCM. *Atmos Ocean Sci Lett* 7:1–6
- Zar J (1998) *Biostatistical analysis*, 4th edn. Pearson Education, Boston
- Zhao P, Chen LX (2001) Interannual variability of atmospheric heat source/sink over the Qinghai-Xizang (Tibetan) Plateau and its relation to circulation. *Adv Atmos Sci* 18:106–116
- Zhao P, Zhang X, Zhou X, Ikeda M, Yin Y (2004) The sea ice extent anomaly in the North Pacific and its impact on the East Asian summer monsoon rainfall. *J Clim* 17:3434–3447
- Zhao P, Zhou ZJ, Liu JP (2007) Variability of Tibetan spring snow and its associations with the hemispheric extratropical circulation and East Asian summer monsoon rainfall: an observational investigation. *J Clim* 20:3942–3955
- Zhou L, Liu Y, Bao Q (2012) Computational performance of the high-resolution atmospheric model FAMIL. *Atmos Ocean Sci Lett* 5:355–359
- Zhou XJ, Zhao P, Chen JM, Chen LX, Li WL (2009) Impacts of thermodynamic processes over the Tibetan Plateau on the Northern Hemispheric climate. *Earth Sci* 39:1473–1486. doi:[10.1007/s11430-009-0194-9](https://doi.org/10.1007/s11430-009-0194-9)
- Zhou L, Bao Q, Liu Y, Wu G, Wang WC, Wang X, He B, Yu H, Li J (2015) Global energy and water balance: characteristics from finite-volume atmospheric model of the IAP/LASG (FAMIL1). *J Adv Model Earth Syst.* doi:[10.1002/2014MS000349](https://doi.org/10.1002/2014MS000349)
- Zhu Y (2009) The Antarctic oscillation-East Asian summer monsoon connections in NCEP-1 and ERA-40. *Adv Atmos Sci* 26:707–716
- Zhu Z, Li T, He J (2014) Out-of-phase relationship between boreal spring and summer decadal rainfall changes in southern China. *J Clim* 27:1083–1099